1. SUPPLEMENTAL MATERIAL

1. The mean field

The bare mean field is taken to be a Saxon-Woods potential containing a central and a spin-orbit term as in [1] (see Eq. (2-180)) :

$$V(r) = V_{WS} f(r) + V_{ls}(\vec{l}\cdot\vec{s}) r_0^2 \frac{1}{r}\frac{df(r)}{dr}, \tag{1}$$

with

$$f(r) = \left[1 + \exp\left(\frac{r - R_{WS}}{a_{WS}}\right)\right]^{-1}. \tag{2}$$

The kinetic term is written as $T = -\frac{\hbar^2}{2}\vec{\nabla}\frac{1}{m_k(r)}\vec{\nabla}$, where the $k-$mass has been parameterised according to,

$$m_k(r) = m_{red} - 0.2\left[1 + \exp\left(\frac{r - R_m}{a_m}\right)\right]^{-1}, \tag{3}$$

with a_m = 0.5 fm, R_m = 2.34 fm. Far from the nucleus, the effective mass becomes equal to the reduced mass, $m_{red} = 10/11 = 0.91m$, while at the origin $m_k = 0.71m$. This parameterization is chosen so as to simulate the radial dependence associated with the mean field obtained with the Skyrme SGII effective interaction (see below Section 4).

The parameters of the central potential have been varied so that the solution of the Dyson equation in a box of radius R_{box} = 50 fm reproduces the experimental energies after renormalization ((NFT)$_{ren}$ dressing). We include a constraint on the value of the quantity $\delta_n V_{WS} = \beta_2^n R_{WS} V_{WS}$, which is varied around the average experimental value $\delta_n V_{WS}$ = 119 MeV fm, determined by electromagnetic decay and proton inelastic scattering (see Sect. 2). The deviation from theoretical output and experiment to be minimized is then

$$\begin{aligned}\chi^2 = (\tilde{\epsilon}_{s_{1/2}} - \epsilon^{exp}_{s_{1/2}})^2 + (\tilde{\epsilon}_{p_{1/2}} - \epsilon^{exp}_{p_{1/2}})^2 + (\tilde{\epsilon}_{d_{5/2}} - \epsilon^{exp}_{d_{5/2}})^2 \\ +(0.15 \times (\tilde{\epsilon}_{p_{3/2}} - \epsilon^{exp}_{p_{3/2}}))^2 + (0.01 \times (\beta_2^n V_{WS} R_{WS} - 119 \text{ MeV fm}))^2,\end{aligned} \tag{4}$$

where $\epsilon^{exp}_{s_{1/2}}$= -0.502 MeV, $\epsilon^{exp}_{p_{1/2}}$ = -0.182 MeV, $\epsilon^{exp}_{d_{5/2}}$ = +1.281 MeV and $\epsilon^{exp}_{p_{3/2}}$ = -6.81 MeV.

We have normalized the differences between theory and experiment, so that a similar relative error for the various quantities has a similar impact on the value of χ^2. We have also required the admixture of the 2^+ phonon in the wave function of the dressed $\widetilde{1/2^+}$, $\widetilde{1/2^-}$ and $\widetilde{5/2^+}$ states to be larger than 10%.

In this Supplemental material, we also take into account the coupling with octupole vibrations and with monopole pairing vibrational modes, which are discussed below in Sect. 2 and 3. It will be shown in Sect. 4 that the effect of these couplings is marginal and that it can be effectively taken into account by a slight renormalization of the mean field parameters. Therefore, these couplings have not been been considered in the main text for the sake of a clearer presentation of the essential physical picture.

2. Coupling to surface vibrations

The quadrupole collective vibrations of the system are calculated within the RPA, using a separable interaction with a coupling constant tuned to reproduce the energy and transition strength of the lowest 2^+ state, which plays the dominant role in the renormalisation processes. For the octupole vibrations the standard self consistent coupling strength [2] has been employed. The basic matrix element connecting single-particle level $a \equiv \{nlj\}$ with an intermediate particle-phonon state $b\lambda\nu$, where $\lambda\nu$ denotes a collective surface vibration associated with a deformation parameter $\beta_{\lambda\nu}$, is calculated as in [2] (see Eq. (6-209)):

$$h(a, b\lambda\nu) = -i^{l_a+\lambda-l_b} \left(\frac{1}{\sqrt{4\pi}}\right)^{1/2} < j_a \frac{1}{2} \lambda 0 | j_b \frac{1}{2} > \beta_{\lambda\nu} \int dr r \frac{dV}{dr} \phi_a(r) \phi_b(r). \tag{5}$$

We note that the details of the microscopic calculations do not play a relevant role in the present case. In fact, we only need the energy and the deformation parameters of the vibrations, and in practice we have used the experimental values for the lowest quadrupole vibrational state. The RPA spectrum has been used for the higher quadrupole modes and for the octupole modes.

A 2^+ low-lying state is found in ^{10}Be at E= 3.37 MeV. It has a value of $B(E2\uparrow) = 52 \pm 6$ e^2 fm^4, which corresponds to $\beta_2^{em} = 1.13$, to 8.1 s.p.u. and to the electromagnetic deformation length $\delta^{em} = \frac{M_p}{Z} = 2.92 \pm 0.17$ fm [3] . This state was excited by proton inelastic scattering [4]. The resulting proton deformation length is $\delta_p = \beta_2 R = 1.80 \pm 0.25$ fm. One can then get an estimate of the neutron deformation length using the model by Bernstein which is often employed in the analysis of inelastic scattering [5]:

$$\delta_p = \frac{0.3M_p + 0.7M_n}{0.3Z + 0.7N} \quad ; \quad \delta_n = \frac{0.7M_p + 0.3M_n}{0.7Z + 0.3N} \quad ; \tag{6}$$

from where one obtains $\delta_n = 2.38 \pm 0.35$ fm, which for standard values of R correspond to $\beta_2^n \approx 0.9$. The depth of the neutron central potential used in the experimental analysis by

Iwasaki et al. is $V_n = 50.3$ MeV, leading to $\delta_n V_n = 119 \pm 18$ MeV fm, which is the value that we take as an empirical input to be used in our calculations (see Section 1).

3. Coupling to pair vibrations

Monopole pair addition and removal modes have been calculated within pp-RPA, using the Gogny interaction [6]. Denoting the matrix elements of the interaction between antisymmetrized pairs of states coupled to angular momentum and parity equal to 0^+ by $G_{aa';bb'}$, the pairing mode wave functions are obtained solving the equations

$$\begin{aligned}(\epsilon_k + \epsilon_{k'})X_{kk'} - \sum_{p\leq p'} G_{kk';pp'}X_{pp'} - \sum_{h\leq h'} G_{kk';hh'}X_{hh'} = EX_{kk'} \\ (\epsilon_i + \epsilon_{i'})X_{ii'} + \sum_{p\leq p'} G_{ii';pp'}X_{pp'} + \sum_{h\leq h'} G_{ii';hh'}X_{hh'} = EX_{ii'},\end{aligned} \tag{7}$$

where occupied (unoccupied) orbitals have been labeled by h, i and by k, p respectively. Pair addition (removal modes) are characterized by the dominance of amplitudes over unoccupied (occupied) states. The normalisation is given by

$$\sum_{p\leq p'} X^2_{pp'} - \sum_{h\leq h'} X^2_{hh'} = \pm 1, \tag{8}$$

where the minus sign applies to removal modes. In this paper we only consider the renormalisation of particle states, which couple to the pair removal mode. We will take into account only the lowest mode, which will be denoted $0^{(-)}$, with energy $\hbar\omega^{rem}$. The coupling vertex between a particle a and the $b0^{(-)}$ configuration is given in this case by

$$h(a, b0^{(-)}) = \frac{\delta_{j_a j_b}\delta_{l_a l_b}}{\sqrt{2j_a + 1}} \sum_{cc'} X_{cc'}G_{ab;cc'}. \tag{9}$$

The values of G have been multiplied by a factor equal to 0.85, in order to precisely reproduce the absolute value of the experimental two-neutron separation energy. The calculated amplitudes of the lowest pair removal mode are reported in Table SI.

E(MeV)	$X_{1s_{1/2}}$	$X_{p_{3/2}}$	$Y_{2s_{1/2}}$	$Y_{p1/2}$	$Y_{d_{5/2}}$
-8.48	0.20	1.28	0.21	0.53	0.59

Table SI: Energy and wavefunction of the lowest removal mode $0^{(-)}$, used to renormalize the $s_{1/2}, p_{1/2}$ and $d_{5/2}$ particle states.

4. Calculation of the single-particle energies and spectroscopic amplitudes

The matrix elements of the self-energy matrix $\Sigma_{i,k}(E)$ between a pair of single-particle states of ^{11}Be labeled $i \equiv \{n_i, l_i, j_i\}$, $k \equiv \{n_k, l_k, j_k\}$ and of energies $(\epsilon_i, \epsilon_k > \epsilon_F)$ are written as,

$$\Sigma_{i,k}(E) = \delta_{l_i,l_k}\delta_{j_i,j_k}[\delta_{n_i,n_k}\epsilon_{n_i lj} + \Sigma^{pair}_{i,k}(E) + \Sigma^{surf}_{i,k}(E)], \tag{10}$$

where the contribution associated with the coupling to surface vibrations is given by

$$\Sigma^{surf}_{i,k}(E) = \sum_{\lambda,\nu,c,\epsilon_c>\epsilon_F} \frac{h(i,c\lambda\nu)h(k,c\lambda\nu)}{E-(\epsilon_c+\hbar\omega_{\lambda,\nu})} + \sum_{\lambda,\nu,c,\epsilon_c<\epsilon_F} \frac{h(i,c\lambda\nu)h(k,c\lambda\nu)}{E-(\epsilon_c-\hbar\omega_{\lambda,\nu})} \tag{11}$$

and that associated with the coupling to the lowest pair vibrational state by

$$\Sigma^{pair}_{i,k}(E) = \sum_{\lambda,n,c,\epsilon_c>\epsilon_F} \frac{h(i,c0^{(-)})h(k,c0^{(-)})}{E+(\epsilon_c-\hbar\omega^{rem})}. \tag{12}$$

The sum is taken over the phonons λ, ν and over a set of intermediate states $c \equiv \{n_c l_c j_c\}$.

We include in the calculations particle states of angular momentum $s_{1/2}, p_{1/2}$ and $d_{5/2}$ up to an energy cut off $E_{cut} = 25$ MeV. We include a single hole state, namely the $1p_{3/2}$ orbital. The self-energy matrix is diagonalized separately for each l, j, on an energy mesh, and the resulting eigenvalues $\tilde{\epsilon}_{lj,n}$ are a solution of the Dyson equation,

$$\sum_k [\Sigma_{i,k}(\tilde{\epsilon}_{lj,n}) \times x^{lj}_k] = \tilde{\epsilon}_{lj,n} x^{lj}_i. \tag{13}$$

A given solution has a single-particle component and a collective part. Denoting the eigenvectors by x^{lj}_i (normalised so that $\sum_i (x^{lj}_i)^2 = 1$) , the single-particle component is written as

$$\tilde{\phi}_{lj}(r) = \sum_{n_i} x^{lj}_i \phi_{n_i lj}(r), \tag{14}$$

while the component of the collective part associated with a given particle-phonon configurations $c, \lambda n$ is given by

$$\tilde{\phi}^{c,\lambda\nu}_{lj}(r) = \sum_{n_c} R_{(c,\lambda\nu)_{lj}} \phi_{n_c l_c j_c}(r), \tag{15}$$

where $R_{(c,\lambda\nu)_{lj}} = \sum_i x_i^{lj} \frac{h(i,c\lambda\nu)}{\tilde{\epsilon}_{lj,i}-(\epsilon_c+\hbar\omega_{\lambda\nu})}$ for $\epsilon_c > \epsilon_F$ and $R_{(c,\lambda\nu)_{lj}} = \sum_i x_i^{lj} \frac{h(i,c\lambda\nu)}{\tilde{\epsilon}_{lj,i}-(\epsilon_c-\hbar\omega_{\lambda\nu})}$ for $\epsilon_c < \epsilon_F$. The square of the single particle component of the dressed state is then given by

$$a_{lj}^2 = \frac{1}{1+\sum_{c',\lambda'\nu'}(R_{(c',\lambda'\nu')_{lj}})^2} \tag{16}$$

while the admixture of the solution with the $c, \lambda\nu$ configuration is given by

$$a_{(c,\lambda\nu)_{lj}}^2 = \frac{(R_{(c,\lambda\nu)_{lj}})^2}{1+\sum_{c',\lambda',\nu'}(R_{(c',\lambda'\nu')_{lj}})^2} \tag{17}$$

The above solution provides the first term of the series of rainbow diagrams dressing the single-particle states, taking into account the effect of many-phonon configurations. Higher order terms can be generated iterating the solution self-consistently [7]. We have not attempted to perform such a calculation in the present paper, but employ empirical renormalisation, choosing the single-particle intermediate states so as to reproduce the (low-lying) experimental energies, and eventually the outcome of the clothing process, i.e. $\tilde{\epsilon}_{lj}$ and $\tilde{\phi}_{lj}$. In other words, the solution of the Dyson equation will be acceptable only if the single-particle component of the solution is in agreement with the input used for the intermediate basis, a requirement imposing a severe self-consistent condition to our diagonalization process. In the calculations we have added a correction to the energy of the intermediate particle-phonon configurations, to correct for Pauli principle violation associated with many-phonon states (anharmonicities, see Section 6), implicitly considered in the empirical renormalization. Such corrections are particularly important in the case of the renormalization of the $d_{5/2}$ states, because of the conspicuous coupling to the $s_{1/2} \otimes 2^+$ configuration.

The optimal deformation parameters and geometrical mean field parameters obtained from our fitting procedure are shown in Table SII. Also shown is the value of the product $\beta_2^n R_{WS} V_{WS}$, which is very close to the average experimental value 119 MeV fm.

The radial dependence of the central term of the resulting Saxon-Woods potential and of the associated effective mass (see Eq.(3)) are shown in Fig. S1They closely resemble the corresponding quantities obtained from a Hartree-Fock calculation with the SGII interaction, also shown in Fig.S1. Actually, using directly the SGII mean field in the $(\mathrm{NFT})_{ren}$ calculation, the energies of the $\widetilde{1/2^+}$ and of the $\widetilde{1/2^-}$ renormalised states turn out to be close to the experimental values, while the energy of the $\widetilde{5/2^+}$ resonance is too low.

The energies of the dressed $\widetilde{1/2^+}, \widetilde{1/2^-}$ and $\widetilde{5/2^+}$ resulting from the fit are reported in Table SIII. In each case, the results obtained including or excluding (as in the main text) the

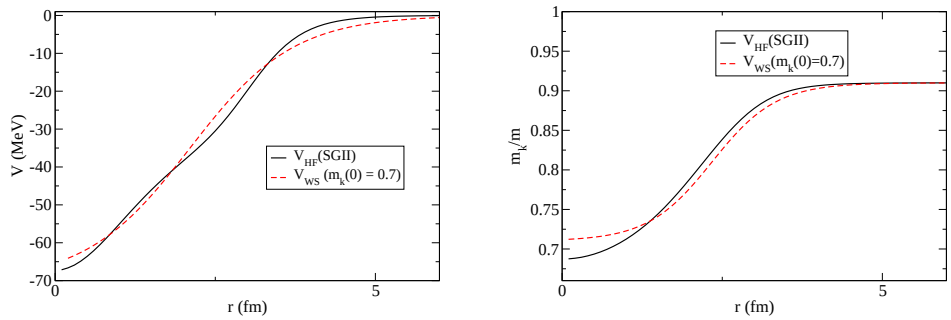

Fig S1: The central potential (left panel) and the effective mass (right panel) calculated with the fitted Saxon-Woods potential (including the coupling to couple and pairing vibrations) are compared to the corresponding quantities obtained from a Hartree-Fock calculation with the SGII Skyrme interaction.

couplings to octupole (oct.) and pairing vibrations (p.v.) are compared. The wavefunctions of the lowest dressed states including the coupling to octupole and pairing vibrations are given by

$$\begin{aligned}
|\widetilde{1/2^+}\rangle &= \sqrt{0.82}|s_{1/2}\rangle + \sqrt{0.17}|(d_{5/2}\otimes 2^+)_{1/2^+}\rangle \\
&\quad + \sqrt{0.01}|(s^2_{1/2}(0)\otimes 0^{(-)})s_{1/2}\rangle \qquad (18)\\
|\widetilde{1/2^-}\rangle &= \sqrt{0.84}|p_{1/2}\rangle + \sqrt{0.02}|(d_{5/2}\otimes 3^-)_{1/2^-}\rangle \\
&\quad + \sqrt{0.14}|((p_{1/2},p^{-1}_{3/2})_{2^+}\otimes 2^+)_{0+},p_{1/2}\rangle \qquad (19)\\
|\widetilde{5/2^+}\rangle &= \sqrt{0.56}|d_{5/2}\rangle + \sqrt{0.21}|(s_{1/2}\otimes 2^+)_{5/2^+}\rangle \\
&\quad + \quad \sqrt{0.22}|(d_{5/2}\otimes 2^+)_{5/2^+}\rangle + \sqrt{0.002}|(p_{1/2}\otimes 3^-)_{5/2^+}\rangle \\
&\quad + \sqrt{0.0005}|((d_{5/2},p^{-1}_{3/2})_{3^-}\otimes 3^-)_{0+},d_{5/2}\rangle + \sqrt{0.003}|(d^2_{5/2}(0)\otimes 0^{(-)})_{0^+},d_{5/2}\rangle. \qquad (20)
\end{aligned}$$

They should be compared to those given in Eqs. (1-3) of the main text, obtained without the coupling to octupole and pairing vibrations. These couplings mostly act on the energy of the $1/2^-$ configuration, but with opposite sign, so that their final effect is small.

The renormalised $5/2^+$ phase shifts, displaying a resonance at $E_{res} = 1.25$ (1.45) MeV of width $\Gamma = 140$ keV (170 keV) with (without) coupling to octupole and pair vibrations, are shown in Fig. S2, where they are compared with the phase shifts calculated with the bare potential, displaying a broad resonance at E= 5.5 (7.3) MeV.

The $2s_{1/2}$ orbital is not bound in our initial bare potential. As a consequence, using the

	β_2^n	β_3^n	V_{WS}	V_{ls}	a_{WS}	R_{WS}	$\beta_2^n R_{WS} V_{WS}$
With oct. and p.v. coupling	0.77	0.28	70.2	0.31	0.81	2.10	115
No oct. and no p.v. coupling	0.79	-	68.9	0.21	0.77	2.15	119

Table SII: Optimal values of the deformation parameters β_2^n, β_3^n, and of the depth, radius, diffuseness and spin-orbit strength of the mean field potential V_{WS}, V_{ls} (in MeV), a_{WS}, R_{WS} (in fm). Finally, we give the value of the product $\beta_2^n R_{WS} V_{WS}$ (in MeV fm).

	$\epsilon_{p_{3/2}}$	$\epsilon_{p_{1/2}}$	$\tilde{\epsilon}_{p_{1/2}}$	$S(1/2^-)$	$\epsilon_{s_{1/2}}$	$\tilde{\epsilon}_{s_{1/2}}$	$S(1/2^+)$	$\epsilon^{res}_{d_{5/2}}$	$\tilde{\epsilon}^{res}_{d_{5/2}}$
With oct. and p.v. coupling	-6.84	-2.21	-0.18	0.84	0.06	-0.50	0.82	5.50	1.25
No oct. and no p.v. coupling	-6.37	-3.04	-0.18	0.84	0.07	-0.50	0.80	7.30	1.47

Table SIII: Unperturbed energies $\epsilon_{p_{3/2}}$, $\epsilon_{p_{1/2}}$ and $\epsilon_{s_{1/2}}$, renormalized energies $\tilde{\epsilon}_{p_{1/2}}$ and $\tilde{\epsilon}_{s_{1/2}}$, resonant single-particle energies $\epsilon^{res}_{d_{5/2}}$, renormalised resonant energies $\tilde{\epsilon}^{res}_{d_{5/2}}$ (all in MeV), spectroscopic factors $S(1/2^-)$ and $S(1/2^+)$, obtained with the optimal values reported in Table SII.

same basis for the asymptotic and the intermediate states, the coupling matrix element will be small due to the poor overlap in the corresponding radial wavefunctions. Iterating the diagonalization, the $s_{1/2}$ state eventually becomes bound, acquiring in the process a collective component of the type $d_{5/2} \otimes 2^+$. At the same time, $5/2^+$ states will acquire both a bound collective component through the coupling with the $s_{1/2} \otimes 2^+$ configuration and a localized (resonant) single-particle wave function due to the mixing of the various continuum states. For economy, these processes are taken into account within the framework of empirical renormalization using a (intermediate) $s_{1/2}$ state bound by 0.5 MeV as in experiment, and verifying that this value coincides with the energy $\tilde{\epsilon}_{1/2^+}$ of the final dressed $|\widetilde{1/2^+}>$ state.

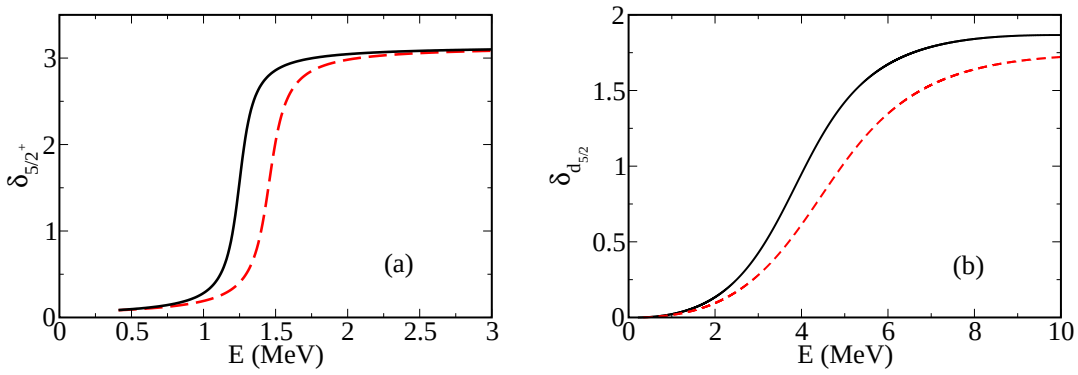

Fig. S2: (a) $5/2^+$ $(\mathrm{NFT})_{ren}$ phase shifts as a function of energy, with (solid line) or without (dashed line) the coupling to octupole and pairing vibration modes. (b) $d_{5/2}$ phase shifts calculated with the corresponding bare potentials (see Table II).

5. Bubble overcounting

Freely summing over intermediate particle $\otimes$ phonon configurations when evaluating the self-energy diagrams, leads as a rule to some overcounting, since phonons are linear combinations of particle-hole configurations (see Fig. S3).

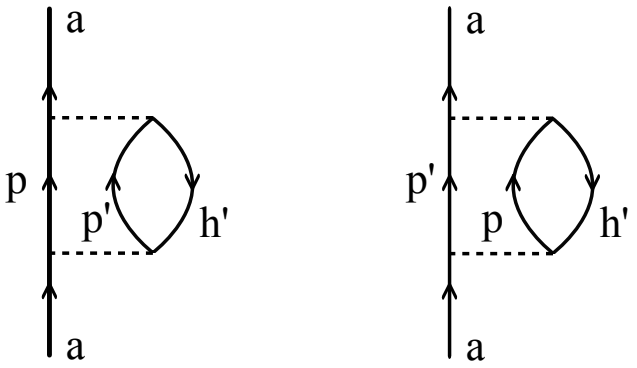

Fig. S3: The diagram at the right contains the same intermediate configuration as that of the left one. If antisymmetrised two-body matrix elements are used, these two diagrams are identical.

Such overcounting can be cured subtracting the overcounted bubble diagram from the particle-phonon (RPA series) calculation. In the present case, such overcounting is small (a few per cent, smaller than our global theoretical accuracy). In fact, the low lying 2^+ phonon, which is by far the most relevant phonon in our calculations, is constructed mostly out of particle-hole transitions between single-particle states of negative parity ($1p^{-1}_{3/2}$ holes; $p_{1/2}$ (mainly), $p_{3/2}$ (very little), $f_{7/2}$ and $f_{5/2}$ (negligibly) particles) and marginally by particle-hole transitions of positive parity ($1s^{-1}_{1/2}$ holes, $d_{5/2}$ and $d_{3/2}$ particles). When evaluating the (positive parity) self-energies of the $s_{1/2}$ and $d_{5/2}$ states, the intermediate $p\otimes 2^+$ configuration involves particle states of positive parity, and as a consequence overcounting is produced only by the small positive parity particle-hole components of the 2^+ phonon (see Fig. S4). On the other hand when evaluating the (negative parity) $p_{1/2}$ self-energy no overcounting arises since only one $p_{3/2}$ hole contributes and no involved summation can lead to overcounting (see Fig. S4).

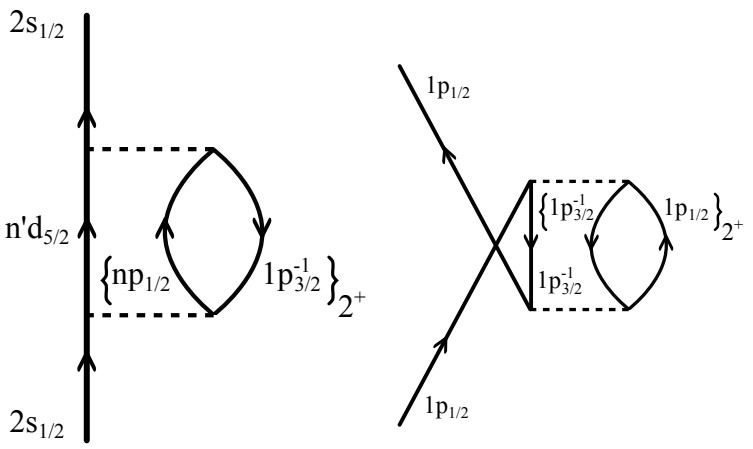

Fig. S4: (left) Main p'-h' configuration renormalizing the $2s_{1/2}$ state. Summing over the number of nodes n and n' does not lead to double counting, in keeping with the different parity and angular momentum of the $d_{5/2}$ and $p_{1/2}$ states. An identical reasoning applies to the $5/2^+$ states. (right) Main p'-h' configuration renormalizing the $1p_{1/2}$ state. In this case only the $1p^{-1}_{3/2}$ hole state is taken into account, and no overcounting is possible.

6. Anharmonic effects

An important point concerns anharmonic effects in many-phonon configurations, associated with the Pauli principle, which are not taken into account in the rainbow series. They are particularly relevant in the present case due to the low angular moment of the single-particle states involved in the calculation. The intermediate configurations $\tilde{d}_{5/2} \otimes 2^+$ and $\tilde{s}_{1/2} \otimes 2^+$ (see Fig. 2, panels (I)(a) and (III)(a),(b) in the main text) implicitly contain a 2-phonon component and this involves an anharmonic effect associated with violation of the Pauli principle. In NFT the Pauli principle is restored by the so called butterfly diagrams (and associated ones, see [8], Eqs. (28-35)), which take into account the fermion exchange between the microscopic p-h structures of the involved phonons (see Fig. S5). We have not calculated in detail the diagrams but we have estimated the associated correction by performing a RPA calculation blocking the relevant p-h transitions. This is an approximate method which coincides with the exact evaluation of the butterfly diagram in the two-level model. We obtain an increase of the energy of the two-phonon configuration of 2.7 MeV and a reduction of the deformation parameter β_2 of about 30%. The influence of these changes on the empirical-particle-phonon configurations energy depends on how much two-phonon weight they carry, which in turn is an output of our calculations. A consistent calculation leads to an increase of about 2 MeV for the $d_{5/2} \otimes 2^+$ configuration and of about 1 MeV for the $s_{1/2} \otimes 2^+$ one (see Fig. S5). The difference between these two corrections reflects the fact that the calculated 2^+ phonon admixture in the dressed $5/2^+$ state (50%) is about twice the value obtained for the $1/2^+$ state (20%).

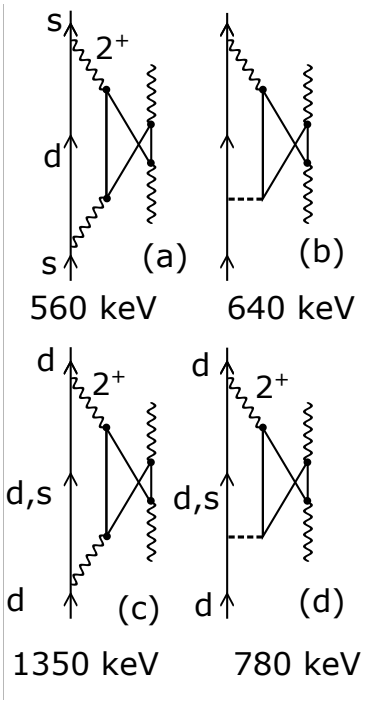

Fig. S5: Butterfly diagrams taking care of the Pauli principle violation of the two phonon states implicitly appearing in the intermediate states $\tilde{s}_{1/2} \otimes 2^+$ and $\tilde{d}_{5/2} \otimes 2^+$.

7. Calculation of the dipole matrix element

The measured value of the transition strength associated with the dipole transition between the first excited state and the ground state of ^{11}Be is $B(E1) = 0.102 \pm 0.02$ e^2 fm^2 = 0.32 W.U. [9]. The transition strength is defined as

$$B(E1; I_i \to I_f) = \frac{1}{2I_i + 1} | < I_f || iM(E1) || I_1 > |^2 \tag{21}$$

The leading contribution for the $1/2^+ \to 1/2^-$ transition is obtained calculating the transition between the single-particle part of the renormalised wave functions, weighted with the appropriate single-particle factor and multiplied by the recoil effective charge $e_{eff} = -eZ/A = -4e/11$:

$$B(E1; I_i \to I_f) = \frac{e_{eff}^2}{2I_i + 1} \widetilde{a^2_{1/2^+}} \widetilde{a^2_{1/2^-}} |M^0|^2 \tag{22}$$

where

$$M^0 \equiv < 1/2^- || iM(E1) || 1/2^+ > = \sqrt{\frac{3}{2\pi}} \frac{-1}{\sqrt{3}} I(E1) = -\sqrt{\frac{1}{2\pi}} I(E1), \tag{23}$$

with $I(E1) = \int dr \tilde{\phi}_{1/2^+}(r) r \tilde{\phi}_{1/2^-}(r)$. The amplitudes are equal to $\widetilde{a^2_{1/2^+}} = 0.80$ and $\widetilde{a^2_{1/2^-}} = 0.84$ (see Eqs.(1) and (2) of the main text). Numerically one finds $I(E1) \approx 5$ fm, leading to the zero-order result

$$B(E1; 1/2^+ \to 1/2^-) \approx \frac{16}{121} \frac{1}{2} 0.67 \frac{1}{2\pi} 25 \quad \text{e}^2\text{fm}^2 = 0.17 \text{e}^2\text{fm}^2. \tag{24}$$

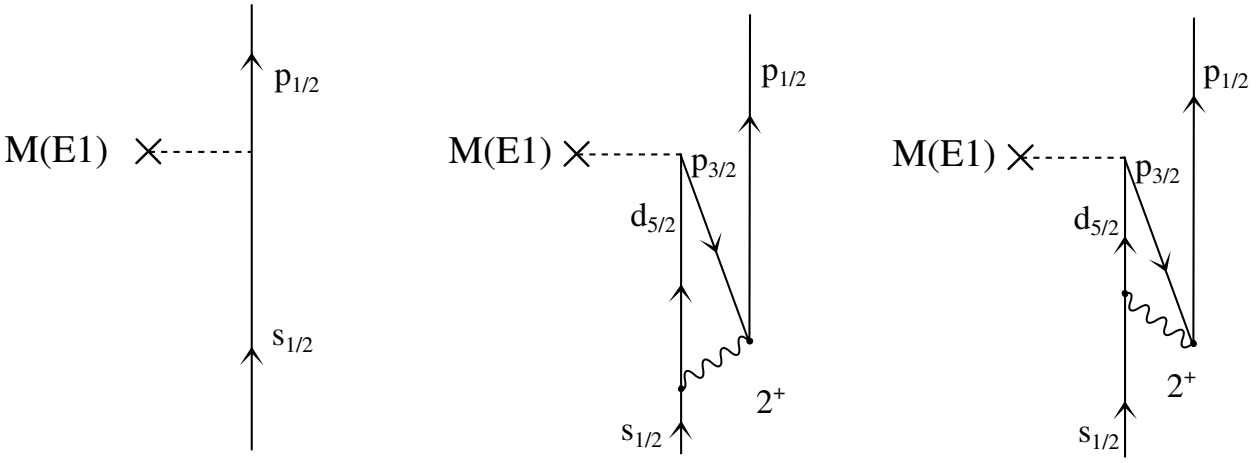

Fig. S6: Main processes contributing to the dipole transition between the first excited state and the ground state of ^{11}Be. The vertex correction associated with the low-lying 1^- strength (incipient GDPR) is estimated to be small.

One has to consider, however, that one expects other important contributions from many-body processes. The two time orderings associated with the most important ones are shown in the right part of Fig. S6. They interfere in a destructive way with the leading contribution, leading to

$$B(E1; I_i \to I_f) = \frac{e_{eff}^2}{2I_i+1} a_{1/2^+}^2 a_{1/2^-}^2 |M^0 + M^{1(a)} + M^{1(b)}|^2$$

$$= \frac{16}{121}\frac{1}{2} 0.67 |\sqrt{\frac{1}{2\pi}} \times 5 - 0.28 - 0.19|^2 \quad \mathrm{e^2fm^2} = 0.11 \quad \mathrm{e^2fm^2}. \tag{25}$$

including the coupling to octupole and pairing vibration leads to $B(E1) = 0.12\mathrm{e^2fm^2}$. We remark that the usual depletion of the low-lying E1 strength by the giant resonance is not very effective in the present case, due to the poor overlap between the halo neutron single-particle states and those of the nucleons of the core (see [10], [11], p.2 and App. A,B; see also [12]). In fact, it can be estimated that the contribution of the giant dipole polarisation diagram is much smaller than the bare M(E1) diagram due to the halo character of the wave functions, and that it also much smaller than the second order quadrupole polarisation corrections due to the smaller deformation parameter of the GDR compared to quadrupole mode, and to its much larger excitation energy.

8. Calculation of the charge radius

An estimate of the difference between the value of the charge radius in ^{11}Be and ^{10}Be can be obtained by considering that the dressed $\widetilde{1/2^+}$ wave function has a $s_{1/2}$ single-particle part with amplitude $a_{\widetilde{1/2^+}} = \sqrt{0.80}$ and a collective part dominated by the admixture with the lowest 2^+ vibration of amplitude $a_{(d_{5/2^+}\otimes 2^+)_{1/2^+}} = \sqrt{0.20}$ (see Eq. (1) of the main text). The contribution to the square charge radius due to the single-particle part is due to core recoil:

$$(a_{\widetilde{1/2^+}})^2 \left(< r^2 >_{^{10}Be} + \left(\frac{< r^2 >_{s_{1/2}}^{1/2}}{11} \right)^2 \right) \tag{26}$$

The contribution of the collective part is instead given by

$$a^2_{(d_{5/2^+}\otimes 2^+)_{1/2^+}} \left(< r^2 >_{^{10}Be} (1 + \frac{2}{4\pi}(\beta_2^{em})^2) + \left(\frac{< r^2 >_{(d_{5/2}\otimes 2^+)_{1/2^+}}^{1/2}}{11} \right)^2 \right), \tag{27}$$

where we have used the fact that the mean square radius of the nucleus in its 2^+ state (first excited state of a harmonic oscillator) is a factor $(1 + \frac{2}{4\pi}(\beta_2^{em})^2)$ larger than in its ground

state, while the neutron in the $(d_{5/2^+} \otimes 2^+)_{1/2^+}$ state is described by the wave function $\phi^{d_{5/2},2^+}_{s_{1/2}}$. One then obtains

$$< r^2 >_{^{11}Be} = < r^2 >_{^{10}Be} + (a_{\widetilde{1/2^+}})^2 \left(\frac{< r^2 >^{1/2}_{s_{1/2}}}{11} \right)^2 +$$

$$a^2_{(d_{5/2^+} \otimes 2^+)_{1/2^+}} \left(< r^2 >_{^{10}Be} \frac{2(\beta_2^{em})^2}{4\pi} + \left(\frac{< r^2 >^{1/2}_{(d_{5/2} \otimes 2^+)_{1/2^+}}}{11} \right)^2 \right). \quad (28)$$

Introducing the values $< r^2 >_{^{10}Be} = 5.57\ fm^2$, $(a_{\widetilde{1/2^+}})^2 = 0.80, a^2_{(d_{5/2^+} \otimes 2^+)_{1/2^+}} = 0.20, \beta_2^{em} = 1.13$, $< r^2 >^{1/2}_{s_{1/2}} = 7.1$ fm and $< r^2 >^{1/2}_{(d_{5/2} \otimes 2^+)_{1/2^+}} = 3$ fm one obtains $< r^2 >_{^{11}Be} = 5.57 + 0.80 \times 0.42 + 0.20 \times (1.13 + 0.07) = 6.15$ fm^2, and $(< r^2 >_{^{11}Be})^{1/2} = 2.48$ fm, to be compared with the experimental value 2.466 fm $\pm$ 0.015 [13]. Inserting the values $(a_{1/2^+})^2 = 0.82$ and $a^2_{(d_{5/2^+} \otimes 2^+)_{1/2^+}} = 0.17$, obtained including the coupling to octupole and pairing vibrations (cf. Eq. (17)), leads to 2.47 fm.

9. Coupled equations

An approximate solution of the Schrödinger equation $H\Psi_a = E\Psi_a$ for the wave function of the clothed odd nucleon can be expressed as

$$\Psi_a = [\tilde{\psi}_{l_a j_a} + [\tilde{\psi}^{l_b j_b \lambda}_{l_a j_a} \cdot \Gamma^\dagger_\lambda]_{j_a} - \bar{\tilde{\psi}}_{l_a j_a} - [\bar{\tilde{\psi}}^{l_c j_c \lambda}_{l_a j_a} \cdot \Gamma_\lambda]_{j_a}] \Phi^A_{GS} \quad (29)$$

where Φ^A_{GS} denotes the ground state of the nucleus of even mass number A (containing the correlations needed so that it is the vacuum of the different elementary modes of excitation used as a basis to describe ^{11}Be, i.e. $a_j|\Phi^A_{GS} >= \Gamma_\lambda|\Phi^A_{GS} >= 0$), $\Gamma^\dagger_\lambda$ denotes a general creation operator of a vibrational state (phonon), calculated using e.g. RPA (we will consider for simplicity the coupling to a single phonon λ),

$$\tilde{\psi}_{l_a j_a} = (\tilde{\phi}_{l_a j_a}(r)/r)\Theta_{l_a j_a} \quad (30)$$

creates a particle in l_a, j_a,

$$[\tilde{\psi}^{l_b j_b \lambda}_{l_a j_a} \cdot \Gamma^\dagger_\lambda]_{j_a} = (\tilde{\phi}^{l_b j_b \lambda}_{l_a j_a}(r)/r)[\Theta_{l_b j_b} \cdot \Gamma^\dagger_\lambda]_{j_a} \quad (31)$$

creates a particle-phonon state coupled to j_a and parity $(-1)^{l_a}$,

$$\bar{\tilde{\psi}}_{l_a j_a} = (\bar{\tilde{\phi}}_{l_a j_a}(r)/r)\Theta_{l_a j_a} \quad (32)$$

annihilates a hole in l_a, j_a and

$$[\bar{\tilde{\psi}}^{l_c j_c \lambda}_{l_a j_a} \cdot \Gamma_\lambda]_{j_a} = (\bar{\tilde{\phi}}^{l_c j_c \lambda}_{l_a j_a}(r)/r)[\Theta_{l_c j_c} \cdot \Gamma_\lambda]_{j_a}, \tag{33}$$

annihilates a hole-phonon coupled to j_a and parity $(-1)^{l_a}$. The radial wavefunctions $\tilde{\phi}_{l_a j_a}$ and $\tilde{\phi}^{l_b j_b \lambda}_{l_a j_a}$ must be expanded over a set of single-particle states (HF) lying above the Fermi energy:

$$\tilde{\phi}_{l_a j_a}(r) = \sum_{n_i} x_i^{l_a j_a} \phi^{HF}_{n_i l_a j_a}(r) \quad , \quad \tilde{\phi}^{l_b j_b \lambda}_{l_a j_a}(r) = \sum_{n_b} R_{(b,\lambda)_{j_a}} \phi^{HF}_{n_b l_b j_b}(r); \epsilon^{HF}_{n_i l_a j_a}, \epsilon^{HF}_{n_b l_b j_b} > \epsilon_F \tag{34}$$

while $\bar{\tilde{\phi}}_{l_a j_a}(r)$ and $\bar{\tilde{\phi}}^{l_b j_b \lambda}_{l_a j_a}(r)$ must be expanded over the occupied states:

$$\bar{\tilde{\phi}}_{l_a j_a}(r) = \sum_{n_i} y_i^{l_a j_a} \phi^{HF}_{n_i l_a j_a}(r) \quad , \quad \bar{\tilde{\phi}}^{l_b j_b \lambda}_{l_a j_a}(r) = \sum_{n_c} R_{(c,\lambda)_{j_a}} \phi^{HF}_{n_c l_c j_c}(r); \epsilon^{HF}_{n_i l_a j_a}, \epsilon^{HF}_{n_c l_c j_c} < \epsilon_F. \tag{35}$$

The radial wavefunction $\bar{\tilde{\phi}}^{l_b j_b \lambda}_{l_a j_a}$ accounts for the proper antisymmetrization of the RPA ground state. In fact the RPA ground state contains 2p-2h configurations, what implies that the odd particle will find states inhibited by the Pauli principle also above ϵ_F. Reciprocally the $\bar{\tilde{\phi}}_{l_a j_a}(r)$ wave accounts for the possibility that the impinging particle will find available states below ϵ_F.

It can be shown that the radial wave functions satisfy the coupled equations

$$\begin{aligned}
[-\frac{\hbar^2}{2m}\frac{d^2}{dr^2} + V_a(+0\hbar\omega]\tilde{\phi}_{l_a j_a} + \Xi_{a,b\lambda}(-rdV/dr)\tilde{\phi}^{l_b j_b \lambda}_{l_a j_a} - \Xi_{a,c\lambda}(-rdV/dr)\bar{\tilde{\phi}}^{l_c j_c \lambda}_{l_a j_a} &= E\tilde{\phi}_{l_a j_a} \\
\Xi_{a,b\lambda}(-rdV/dr)\tilde{\phi}_{l_a j_a} + [-\frac{\hbar^2}{2m}\frac{d^2}{dr^2} + V_b + 1\hbar\omega]\tilde{\phi}^{l_b j_b \lambda}_{l_a j_a} - \Xi_{a,b\lambda}(-rdV/dr)\bar{\tilde{\phi}}_{l_a j_a} &= E\tilde{\phi}^{l_b j_b \lambda}_{l_a j_a} \\
\Xi_{a,b\lambda}(-rdV/dr)\tilde{\phi}^{l_b j_b \lambda}_{l_a j_a} - [-\frac{\hbar^2}{2m}\frac{d^2}{dr^2} + V_a + 0\hbar\omega]\bar{\tilde{\phi}}_{l_a j_a} + \Xi_{a,c\lambda}(-rdV/dr)\bar{\tilde{\phi}}^{l_c j_c \lambda}_{l_a j_a} &= -E\bar{\tilde{\phi}}_{l_a j_a} \\
\Xi_{a,c\lambda}(-rdV/dr)\tilde{\phi}_{l_a j_a} + \Xi_{a,c\lambda}(-rdV/dr)\bar{\tilde{\phi}}_{l_a j_a} - [-\frac{\hbar^2}{2m}\frac{d^2}{dr^2} + V_c - 1\hbar\omega]\bar{\tilde{\phi}}^{l_c j_c \lambda}_{l_a j_a} &= -E\bar{\tilde{\phi}}^{l_c j_c \lambda}_{l_a j_a}
\end{aligned} \tag{36}$$

where

$$V_a(r) = V(r) + V_{ls}(r) + V_{cent}(r) \tag{37}$$

and (see Eq. (5))

$$\begin{aligned}
\Xi_{a,b\lambda} = \langle \Theta_{l_a j_a} \sum_{\lambda\mu} \beta_\lambda Y_{\lambda\mu}[\Gamma^\dagger_{\lambda\mu} + (-1)^\mu \Gamma_{\lambda\mu}][\Theta_{j_b} \cdot \Phi_\lambda]_{j_a} \rangle = \\
-i^{l_a+\lambda-l_b}\left(\frac{1}{\sqrt{4\pi}}\right)^{1/2} < j_a \frac{1}{2} \lambda 0 | j_b \frac{1}{2} > \beta_\lambda
\end{aligned} \tag{38}$$

The conditions (34) and (35) imply that these equations must be solved using projection techniques.

10. Calculation of the absolute differential cross sections

The calculations of the angular distribution of the reaction ^{10}Be(d,p)^{11}Be(J^{π}_f) have been performed in the post representation for the final bound states $J^{\pi}_f = 1/2^+$ and $1/2^-$ while the prior representation has been adopted for the unbound state $5/2^+$, to ensure a rapid convergence. The transfer form factor is obtained from the single-particle component of the many-body wave function. In the case of the $5/2^+$ final state, the ^{10}Be-n potential V_{10Be-n} is also required. We have approximated V_{10Be-n} with the bare Saxon-Woods potential of increased depth (bringing it to V_{WS} = - 90 MeV), so that the associated $d_{5/2}$ elastic phase shift displays a resonance for $\tilde{\epsilon}^{res} \approx 1.45$ MeV. The angular distribution is obtained by summing the cross sections associated with each of the $5/2^+$ eigenstates calculated in a given box and lying in the region of the resonance (discretized continuum). Convergence is obtained for boxes of the order of 40 fm. We note that the cross section associated with each individual peak of energy $\tilde{\epsilon}_n$ approximately represents the value of the cross section integrated over an energy interval lying between $(\tilde{\epsilon}_{n-1} + \tilde{\epsilon}_n)/2$ and $(\tilde{\epsilon}_n + \tilde{\epsilon}_{n+1})/2$. In order to compute the energy distribution $d^2\sigma/dEd\Omega$ for a given value of θ on a sufficiently fine energy mesh, we have adopted a continuum energy distribution with a Voigt shape, fitting the parameters so that the integrals of the distribution best reproduce the values obtained in the different boxes in the appropriate intervals. The resulting distribution has a $FWHM$ of 300 keV. Folding the theoretical calculation with a gaussian curve of $FWHM$ = 220 keV, representing the experimental resolution, estimated from the width of the peaks of the discrete states (cf. Fig. S7), we obtain the line shape shown in the inset of Fig. 1 of the main text, with a $FWHM$ of 400 keV and in good agreement with the experimental results. We note that the experimental cross sections contain a background caused by the other partial waves, that we have not considered in our present calculation. It is remarkable that the experimental width of the energy distribution of the resonance, populated by the ^{10}Be(d,p)^{11}Be($5/2^+$) one-nucleon transfer reaction, is considerably larger than the width associated with the ^{9}Be(t,p)^{11}Be($5/2^+$) two-nucleon transfer reaction (100 keV, see Fig. 1 of the main text) and also larger than that exhibited by the calculated elastic phase shifts (170 keV, see again Fig. 1 of the main text).

Finally, we have also calculated the angular distribution associated with the one-nucleon transfer reaction ^{11}Be(p,d)^{10}Be populating the 2^+ state in ^{10}Be in the post representation,

making use of the collective part $\tilde{\phi}^{d_{5/2},2^+}_{s_{1/2}}$ of the initial $\widetilde{1/2^+}$ state in ^{11}Be (see Sect. 4).

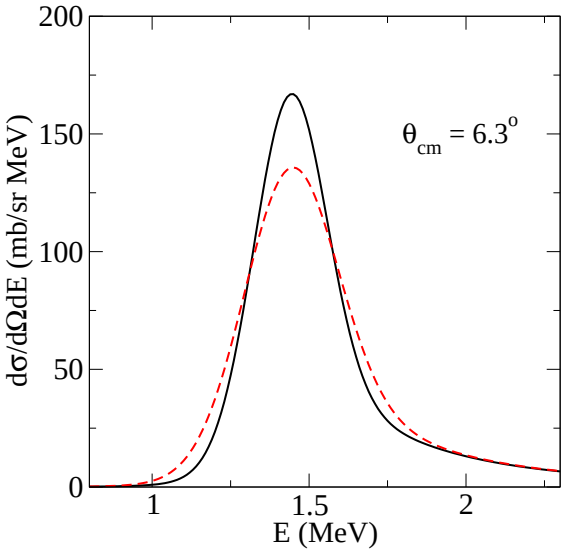

FIg. S7: The theoretical absolute double differential cross section calculated for the reaction ^{10}Be(d,p)^{11}Be populating the $5/2^+$ state at $\theta_{cm} = 6.3^o$ is shown by the solid line. The dashed line shows the result of convoluting this curve with a Gaussian curve of FWHM = 220 keV (estimated experimental resolution).

[1] A.Bohr and B.R.Mottelson, *Nuclear Structure* **Vol. I**, Benjamin, New York (1969)

[2] A.Bohr and B.R.Mottelson, *Nuclear Structure* **Vol. II**, Benjamin, New York (1975)

[3] S. Raman et al., At. Data and Nucl. Data Tables **36** (1987) 1

[4] H.Iwasaki *et al.*, Phys.Lett. B **481** (2000) 7

[5] A.M. Bernstein, V.R. Brown and V.A. Madsen, Phys. Lett. B **103** (1981) 255

[6] G. Blanchon, N. Vinh Mau, A. Bonaccorso, M. Dupuis and N. Pillet, Phys.Rev. C**82** (2010) 034313

[7] A. Idini, F. Barranco and E. Vigezzi, Phys, Rev. **C 85** (2012) 014331

[8] D.R. Bès, R.A. Broglia, G.G. Dussel, R.J. Liotta and H.M. Sofia, Nucl. Phys. A **260** (1976) 1

[9] E. Kwan *et al.*, Phys. Lett. **B732** (2014) 210

[10] F. Barranco, P.F. Bortignon, R.A. Broglia, G. Colò and E. Vigezzi, Eur. Phys. J. A **11** (2001) 385

[11] R.A. Broglia, P.F. Bortignon, F. Barranco, E. Vigezzi, A. Idini and G. Potel, Phys. Scr. **91** (2016) 063012

[12] I. Hamamoto and S. Shimoura, J. Phys. **G34** (2007) 2715

[13] A. Krieger et al., Phys. Rev. Lett. **108** (2012) 142501